Indian Journal of Pure & Applied Physics
Vol. 62, September 2024, pp. 789-805
DOI: 10.56042/ijpap.v62i9.11102

Investigating Effect of Various ETL and HTL on the Solar Cell Parameters of $CsSn_{0.5}Ge_{0.5}I_3$ based lead Free PSC to Obtain Optimized PCE

Nishi Bala[a,b*] & Sanjeev Kumar Mallik[a]

[a]Department of Electrical Engineering, National Institute of Technology, Patna 800 005, Bihar, India

[b]Department of Electrical and Electronics Engineering, Bakhtiyarpur College of Engineering, Champapur, Dedaur, Bakhtiyarpur 803 212, Bihar, India

Received 12 May 2024; accepted 1 August 2024

Wide scale production and commercial uses of PSCs are restricted by the toxicity problems associated with the lead metal, despite the substantial benefits and power conversion efficiency that PSCs have attained over the years. Thus lead-free metal halide perovskites are the focus of modern study. Here the solid-solution perovskite ($CsSn_{0.5}Ge_{0.5}I_3$), an all-inorganic material devoid of lead as the light absorber layer for obtaining high efficiency PSCs is thoroughly investigated. The major objective of present work is to analyze superior combination of ETL and HTL for $CsSn_{0.5}Ge_{0.5}I_3$ for getting affordable, high-efficiency and nontoxic $CsSn_{0.5}Ge_{0.5}I_3$ PSCs. In this work, initially with the use of a one-dimensional solar cell capacitance simulator (SCAPS-1D) thirty-five, $CsSn_{0.5}Ge_{0.5}I_3$ based PSCs were examined which are formed by the combination of seven HTLs and five suitable ETLs including ZnO, TiO_2, WS_2, PCBM and C_{60}. Simulation results showed that among 35 different configurations the device architecture consisting of ITO/WS_2/$CsSn_{0.5}Ge_{0.5}I_3$/PEDOT: PSS/Au had a higher photo conversion efficiency and stability. This configuration provided PCE of 23.47%. For the different possible configurations, the impact of varying the absorber, ETL and HTL width on solar cell parameters was carefully examined. Additionally, the comparison of simulation result obtained by SCAPS-1D software is validated by another simulation software wxAMPS. Further, the effect of series resistance, temperature and shunt resistance has been studied comprehensively for the 5 superior configurations out of the 35 combinations taken.

Keywords: ETL-Electron transport layer, PSC- Perovskite Solar Cell, PAL – Perovskite Absorption Layer, PCE – Power Conversion Efficiency, HTL-Hole transport layer

1 Introduction

Ever-increasing demand of energy and depletion of fossil fuels required the development of alternative source of energy. The solar energy, which is inexhaustible and pro-environment could take lead in tackling future demand of energy. Although silicon solar cells are most widely used in current scenario and its price is par with conventional electricity generation technology, their popularity is somewhat constrained by its expensive fabrication process and strict quality requirements for silicon wafers[1-3].

Perovskite Solar cells of structure ABX3 (Here A is organic/inorganic cation, B is Pb/Sn/Ge cation or their combinations, and X is halide anion or their combinations) has revolutionized the development of photovoltaic technology. The PCE of lead based PSCs rapidly increase over past few years from 3.9% to a certified 25.8%[4-8]. The exceptional optoelectronic characteristics like the high absorption capacity, less carrier binding energy and long diffusion length are attributed for the remarkable increase in PCE[9-10]. But, the toxicity of lead has alarmed concerns for lifecycle of these PSCs, which causes environmental contamination and health issues, a major hurdle in their large scale commercialization and production[11–13]. To combat the toxicity of lead, research is being done on lead-free perovskite materials such Sn, Ge, Sb, Bi and their combinations, as well as other perovskite materials like double perovskites[14]. Therefore, lead-free perovskite materials to replace lead cation is being investigated thoroughly. To replace lead several non-toxic cations having similar properties has been studied by researchers. Sn and Ge cations belongs to same group four of periodic table. Hence Sn and Ge have similar characteristics as of Pb[15-17].

Sn based PSCs show highest PCE because of shorter band gap in comparison to other cations. Typical Sn-based halide perovskites include $MASnI_3$, $FASnI_3$ and $CsSnI_3$. Although it has been demonstrated that $MASnI_3$ and $FASnI_3$ perovskites may achieve good PCE of up to

*Corresponding author: (E-mail: nishijnct@gmail.com)

9%[18], these perovskites are inherently unstable[19-20]. This is mostly owing to the organic cation's presence which is easily volatilized. The $CsSnI_3$ material emerged as an appealing choice in this situation[21]. Further, Sn's +2 oxidation state in fabrication process becomes unstable and quickly oxidises to the +4 state when it gets into touch with air[22-23]. This limits the device's working environment and necessitates the development of new stabilization techniques that can concurrently improve PCE and stability of $CsSnI_3$ based PSCs. To overcome this Ge is alloyed with $CsSnI_3$ to create a perovskite with $CsSn_xGe_{1-x}I_3$ composition, where x ranges from 0 to 1. Min et al. fabricated $CsSn_{0.5}Ge_{0.5}I_3$ taking x=0.5[24]. This alloy perovskite become very stable and air-tolerant. Also $CsSn_{0.5}Ge_{0.5}I_3$'s favorable Goldschmidt tolerance (0.94) and octahedral (0.4) parameters support the structural stability[24]. After Min Chen et.al little work has been done to simulate and fabricate $CsSn_{0.5}Ge_{0.5}I_3$ based PSCs with different combinations of HTL and ETLs.

In the current work, the performance of the lead-free $CsSn_{0.5}Ge_{0.5}I_3$ based PSC is examined thoroughly by utilizing SCAPS-1D (one-dimensional solar cell capacitance simulator). 35 different types of PSCs are simulated and studied by taking seven different HTLs and five different ETLs. ZnO, TiO_2, WS_2, PCBM and C_{60} are used as ETL while Cu_2O, $CuSbS_2$, CuO, P3HT, CFTS, Spiro-OMeTAD and PEDOT: PSS are used as HTL with gold (Au) serving as the back metal contact. Comparative study of each ETL and HTL materials has been done. Impact of the series resistance, shunt resistance, operating temperature, absorber and ETL layer thickness on the characteristics of PSCs has been thoroughly investigated to obtain optimized solar cell parameters. Also J-V and QE characteristics of the best five solar cell has been obtained and the result has been cross validated by another simulator wxAMPS. This work will contribute towards development of efficient and stable $CsSn_{0.5}Ge_{0.5}I_3$ based lead free PSC with compatible HTLs and ETLs, which will further accelerate research in environment friendly PSCs.

By deploying an appropriate ETL and HTL the performance and efficiency of the absorber may be maximized in PSCs. Stability and performance of PSCs are substantially influenced by the characteristics and type of utilized layer material. The valence and conduction band offset are taken into account while choosing appropriate transport layer for the PSCs[25]. Due to their great process ability and tunability HTLs like Spiro-OMeTAD and PEDOT: PSS were often employed by researchers in PSCs[26-27]. However, these materials have limitations because of their instability, low conductivity, and hole transport[28].The ETL should be cost-effective, has a suitable band offset and compatibility with other layers[29].

2 Device structure and Modelling

A lead free PSC has been modelled by using $CsSn_{0.5}Ge_{0.5}I_3$ as absorber layer TiO_2, WS_2, PCBM and C_{60} as ETL while Cu_2O, $CuSbS_2$, CuO, P3HT, CFTS, Spiro-OMeTAD and PEDOT: PSS as HTL, gold (Au) serving as the back metal contact and ITO works as a top electrode. The Proposed PSC devices as shown in Fig. 1(a) are modelled using ITO which works as a top electrode. Thirty-five different

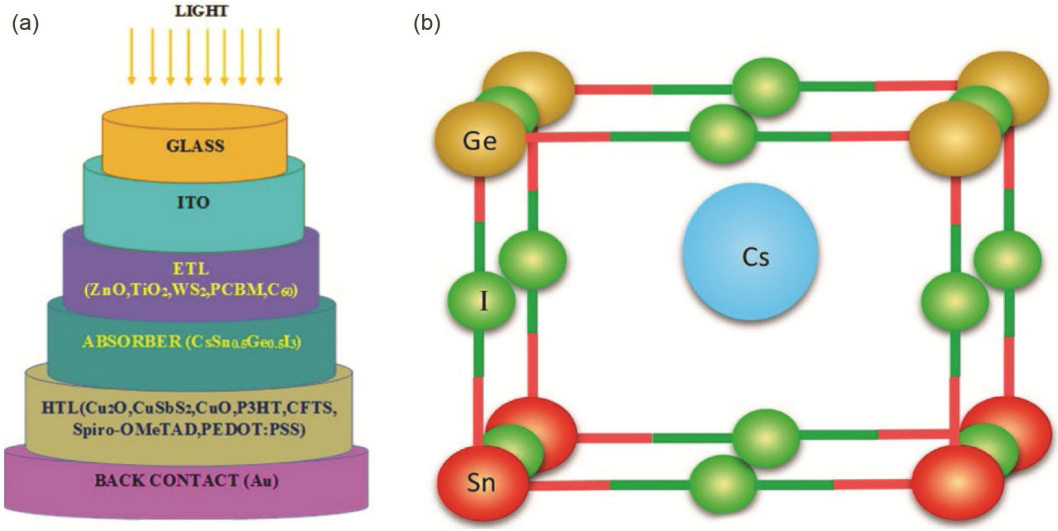

Fig. 1 — (a) Schematic diagram of proposed PSC device (b) Relaxed geometry of $CsSn_{0.5}Ge_{0.5}I_3$ based PSC

combinations of PSCs are simulated and studied by taking different HTLs and different ETLs.

Band offset is very crucial criteria for choosing appropriate transport layer i.e. HTL and ETL. When valance band position of HTL is above with respect to the PAL, it causes significant enhancement in the carrier recombination. While when valence band of the HTL is below with respect to PAL, it causes obstruction in hole transfer and leads incomplete depletion of PAL. Similarly, lower position of conduction band of ETL with respect to the PAL causes a significant enhancement in the interface recombination. While, higher position of the conduction band of the ETL with respect to PAL causes hindrance in electron transfer and leads incomplete depletion of PAL. Fig. 1(b) represents the relaxed geometry of $CsSn_{0.5}Ge_{0.5}I_3$ based PSC where Cs is center of cuboid and Sn and Ge atoms at alternate corner of cuboid.

Figure 2 depicts energy band of the materials with vacuum level utilized in the present study. The PAL absorbs solar spectrum photons whose energy is more than its bandgap and generates electron and hole pairs in the conduction and valance band respectively. Electron moves in conduction band of PAL to ETL which is further collected at ITO. Hole moves in valence band of PAL to HTL and further collected at electrode Au. Generated holes and electrons move towards HTL and ETL respectively. The ETL and HTL are well known for their critical functions. They effectively move charge carriers from the absorber to the appropriate contacts while simultaneously obstructing electron and hole movement towards non desired contacts.

Table 1 shows different interface defect parameters taken for the validation of SCAPS 1D result with the experimental results. Achieving improved efficiency in solar cells is largely dependent on bulk imperfections in the absorber layer. In addition, the PAL/HTL interface and the ETL/PAL interface are crucial problems for PSC operation. ETL serves as a good entry point for extracting electrons from the generic PSC structure, which are impacted by flaws at the ETL/PAL interface.

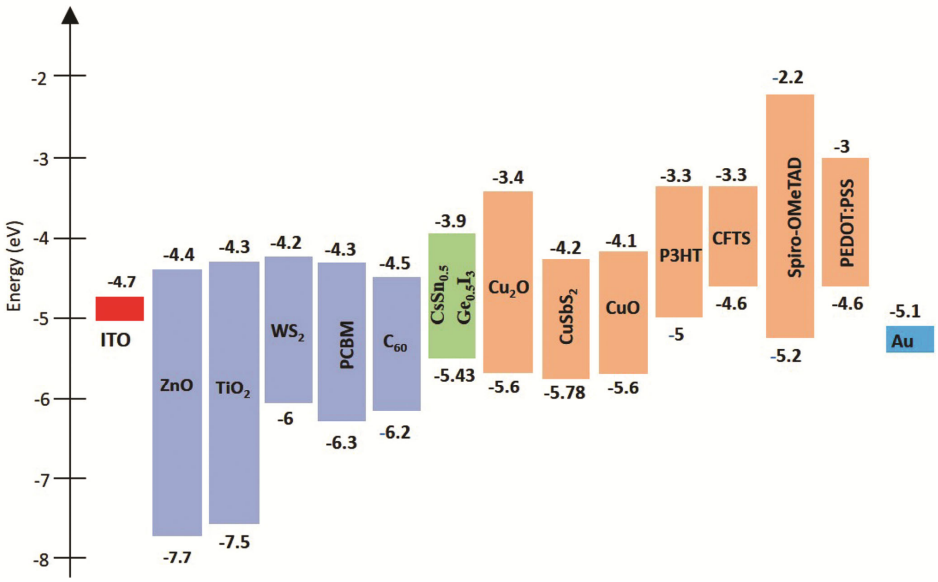

Fig. 2 — Energy band diagram of the materials taken for simulation

Table 1 — The simulation parameters and material properties of layer interface.

Parameters	PCBM / $CsSn_{0.5}Ge_{0.5}I_3$	$CsSn_{0.5}Ge_{0.5}I_3$/ Spiro-OMeTAD
Defect type	neutral	neutral
Electron capture cross section (cm^2)	1×10^{-19}	1×10^{-19}
Hole capture cross section (cm^2)	1×10^{-19}	1×10^{-19}
Energy distribution	Single	Single
Reference for defect energy level	Above E_V (SCAPS<2.7)	Above E_V (SCAPS<2.7)
Energy level with respect to Reference (eV)	0.6	0.6
Total density (integrated over all energies) ($1/cm^2$)	1×10^{10}	1×10^{10}

Likewise, imperfections in the PAL/HTL interface impede the seamless extraction of holes via HTL. The majority of the flaws in the PAL/HTL and ETL/PAL interfaces are caused by a large number of chemical impurities, dangling bonds, uncoordinated atoms and surface dislocations at the PAL surface.

Series resistance is taken as 5 Ω-cm^2, shunt resistance is taken as 1×10^5Ω-cm^2 and temperature as 450 K.

3 Numerical Simulation of SCAPS-1D and wxAMPS

The SCAPS-1D programme solves fundamental semiconductor equations numerically.SCAPS-1D developed by Burgelman primarily used numerical modelling based on four set of electronic device equations, namely Poisson's and Continuity equation.

$$-\frac{d^2\emptyset(x)}{dx^2}=\frac{dE}{dx}=\frac{\rho}{\epsilon}=\frac{q(p-n+N_D^+-N_A^-\pm N_{def})}{\epsilon_0\epsilon_r} \quad \ldots(1)$$

Where$\emptyset$ is electric potential, E is Electric field intensity, ϵ is permittivity, q is charge, n and p are the concentration of electron and hole respectively and ρ is charge density. N_D^+ and N_A^- are concentration of donor and acceptor ions. N_{def} is concentration of defect density of donor and acceptor.

$$-\frac{1}{q}\left(\frac{dJ_e}{dx}\right)=G-R \quad \ldots(2)$$

$$\frac{1}{q}\left(\frac{dJ_n}{dx}\right)=G-R \quad \ldots(3)$$

$\frac{dJ_e}{dx}$ shows variation of electron current density with change in position,

$\frac{dJ_n}{dx}$ is change of hole current density with respect to position,

G is generation and R is recombination rate

The density of state (DOS) model and the longevity model are the two separate models used in the AMPS-1D program. It uses the density of state model to analyze the recombination events, variations of defect states and its effect upon electric field across various layers. The electrostatic potential at every point in the PSC may be found using the AMPS-1D by solving three-coupled non-linear differential equations with suitable boundary conditions. Based on the device depth, the PSC figures of merit may be calculated in line with these variables' definitions. Resolving Poisson's Eq. 4, which connects charge to electrostatic potential and the continuity Eqs 5 & 6 for various device structure areas serve as representations of the device behavior.

$$\frac{d}{dx}\left(\varepsilon(x)\frac{d(\phi(x))}{dx}\right)=e\rho \quad \ldots(4)$$

$$\frac{1}{e}\frac{dJ_N}{dx}=G(x)-R(x) \quad \ldots(5)$$

$$\frac{1}{e}\frac{dJ_P}{dx}=-G(x)+R(x) \quad \ldots(6)$$

where position is indicated by x, dielectric constant by ε, local electric potential by ϕ, electron charge by e, summed charge density by ρ, electron current density by J_N, hole electron density by J_P, optical carrier generation rate by G and overall charge carrier recombination rate by R.

4 Validation with experimental result

Present work is validated by comparing performance of experimental device FTO/PCBM/$CsSn_{0.5}Ge_{0.5}I_3$/ Spiro-OMeTAD /Au as reported by Chen[24] with the performance parameters obtained inSCAPS-1Das well as wxAMPS. Simulated solar cell parameter obtained by SCAPS-1D is shown in Table 2 for the said device.

Table 2 — The simulation parameters and material properties of experimental setup taken in SCAPS[30-32].

Parameters	FTO	$CsSn_{0.5}Ge_{0.5}I_3$	PCBM	Spiro-OMeTAD
Thickness (nm)	500	200 (varied)	50	200
E_g(eV)	3.5	1.5	2	3
Electron Affinity (eV)	4	3.9	3.9	2.2
Relative permittivity	9	28	3.9	3
Conduction band effective density of statesN_c(cm^{-3})	2.2×10^{18}	1×10^{19}	2.5×10^{21}	2.2×10^{18}
Valence band effective density of statesN_v(cm^{-3})	1.8×10^{19}	1×10^{19}	2.5×10^{21}	1.8×10^{19}
Electron thermal velocity (cm/s)	1×10^7	1×10^7	1×10^7	1×10^7
Hole thermal velocity (cm/s)	1×10^7	1×10^7	1×10^7	1×10^7
Electron mobility μ_e (cm^2/Vs)	20	974	0.2	4.5×10^{-2}
Hole mobility μ_h (cm^2/Vs)	10	213	0.2	4.5×10^{-2}
Donor density N_D(cm^{-2})	2×10^{19}	0	2.93×10^{17}	0
Acceptor density N_A(cm^{-2})	0	1×10^9	0	1×10^{18}
N_t(cm^{-3})	1×10^{15}	1×10^{15}	1×10^{14}	1×10^{14}

Table 3 — The comparative solar cell parameters for experimental setup, SCAPS-1D and wxAMPS.

	V_{OC}	J_{SC}	FF	PCE
Experimental	0.63	18.61	60.6	7.11
SCAPS-1D	0.66	18.96	57.7	7.29
wxAMPS	0.78	19.43	63.4	8.34

Table 4 — The simulation parameters and material properties of ITOand different ETLs[30-31].

Parameters	ITO	ZnO	TiO_2	WS_2	PCBM	C_{60}
Thickness (nm)	500	50	30	100	50	50
E_g(eV)	3.5	3.3	3.2	1.8	2	1.7
Electron Affinity (eV)	4	4	4	3.95	3.9	3.9
Relative permittivity	9	9	9	13.6	3.9	4.2
Conduction band effective density of states$N_c(cm^{-3})$	2.2×10^{18}	2.2×10^{18}	2×10^{18}	1×10^{18}	2.5×10^{21}	8×10^{19}
Valence band effective density of states$N_v(cm^{-3})$	1.8×10^{19}	1.9×10^{19}	1.8×10^{19}	2.4×10^{19}	2.5×10^{21}	8×10^{19}
Electron thermal velocity (cm/s)	1×10^{7}	1×10^{7}	1×10^{7}	1×10^{7}	1×10^{7}	1×10^{7}
Hole thermal velocity (cm/s)	1×10^{7}	1×10^{7}	1×10^{7}	1×10^{7}	1×10^{7}	1×10^{7}
Electron mobility μ_e (cm^2/Vs)	20	100	20	100	0.2	8×10^{-2}
Hole mobility μ_h (cm^2/Vs)	10	25	10	100	0.2	3.5×10^{-3}
Donor density $N_D(cm^{-2})$	1×10^{21}	1×10^{18}	9×10^{16}	1×10^{18}	2.93×10^{17}	1×10^{17}
Acceptor density $N_A(cm^{-2})$	0	0	0	0	0	0
$N_t(cm^{-3})$	1×10^{15}	1×10^{14}	1×10^{14}	1×10^{14}	1×10^{14}	1×10^{14}

Result shown by calibrated device nearly matches with experimental one, which validate current work results. Table 3 summarizes the comparative results obtained by the experimental setup and simulations by SCAPS-1D and wxAMPS respectively.

5 Results and Discussion

Different combinations of ETLs, HTLs with $CsSn_{0.5}Ge_{0.5}I_3$ as absorber layer has been studied and simulated for optimum results. ZnO, TiO_2, WS_2, PCBM and C_{60} have been employed as ETL while Cu_2O, $CuSbS_2$, CuO, P3HT, CFTS, Spiro-OMeTAD and PEDOT: PSS employed for HTL. Firstly, each ETL of suitable width is combined with all seven HTL and obtained solar cell parameters for each device. Then they are compared with all other devices. Devices which employed PEDOT: PSS as HTL has shown superior results in comparison to other HTLs. Then after five different PSCs has been designed using PEDOT: PSS as HTL and ZnO, TiO_2, WS_2, PCBM and C_{60} as ETL with $CsSn_{0.5}Ge_{0.5}I_3$ as absorber layer. These devices have been thoroughly investigated for obtaining superior performance solar cells by varying various input parameters. The effect of joint variations of ETL and PAL width on the PSC parameters have been investigated to obtain optimized PSCs. Contour of V_{OC}, J_{SC}, FF and PCE as a joint function of ETL and PAL width is drawn. Optimized result obtained on specific input parameters has been discussed.

5.1. SCAPS 1D Results analysis of the all possible PSCs

From Table 4 & 5 data for all the ETLs and HTLs are utilized for simulations of 35 different PSCs with unique combination of HTL, ETL and $CsSn_{0.5}Ge_{0.5}I_3$ as absorber layer. As such, the result of all 35 different combinations are depicted in Fig. 3. Fig. 3(a-e) shows result of Solar cell parameters V_{OC}, J_{SC}, FF and PCE in bar chart for all HTLs with (a) ZnO (b) TiO_2 (c) WS_2 (d) PCBM and (e) C_{60} as the ETL respectively. Among all HTLs PEDOT: PSS has shown highest efficiency and solar cell parameters with every ETL combinations.

5.2. Energy diagram of $CsSn_{0.5}Ge_{0.5}I_3$ based PSC device with PEDOT: PSS as HTL and ZnO, TiO_2,WS_2, PCBM and C_{60} as ETL

The conduction and valence band offsets (CBO and VBO) have a major effect on the charge movement and directly control device performance. CBO and VBO is defined as follow: -

$CBO = \chi_{Absorber} - \chi_{ETL}$

$VBO = \chi_{HTL} + E_{g\,(HTL)} - (\chi_{Absorber} + E_{g\,(Absorber)})$

Where χ is electron affinity and E_g is band gap of corresponding layers. Numerous research reveal that for smooth conduction and superior solar cell parameters CBO and VBO must be in the range of -0.4eV to +0.4eV.

Table 5 — The simulation parameters and material properties of different HTLs[30].

Parameters	Cu_2O	$CuSbS_2$	CuO	P3HT	CFTS	Spiro-OMeTAD	PEDOT:PSS
Thickness (nm)	100	100	100	50	100	200	50
E_g(eV)	2.2	1.58	1.51	1.7	1.3	3	1.6
Electron Affinity (eV)	3.4	4.2	4.07	3.5	3.3	2.2	3.4
Relative permittivity	7.5	14.6	18.1	3	9	3	3
Conduction band effective density of states $N_c(cm^{-3})$	2×10^{19}	2×10^{18}	2.2×10^{19}	2×10^{21}	2.2×10^{18}	2.2×10^{18}	2.2×10^{18}
Valence band effective density of states $N_v(cm^{-3})$	1×10^{19}	1×10^{19}	5.5×10^{20}	2×10^{21}	1.8×10^{19}	1.8×10^{19}	1.8×10^{19}
Electron thermal velocity (cm/s)	1×10^{7}	1×10^{7}	1×10^{7}	1×10^{7}	1×10^{7}	1×10^{7}	1×10^{7}
Hole thermal velocity (cm/s)	1×10^{7}	1×10^{7}	1×10^{7}	1×10^{7}	1×10^{7}	1×10^{7}	1×10^{7}
Electron mobility $\mu_e(cm^2/Vs)$	200	49	100	1.8×10^{-3}	21.98	4.5×10^{-2}	4.5×10^{-2}
Hole mobility μ_h (cm^2/Vs)	8600	49	0.1	1.86×10^{-2}	21.98	4.5×10^{-2}	4.5×10^{-2}
Donor density N_D (cm^{-2})	0	0	0	0	0	0	0
Acceptor density N_A (cm^{-2})	1×10^{18}	1×10^{18}	1×10^{18}	1×10^{18}	1×10^{18}	1×10^{18}	1×10^{18}
N_t (cm^{-3})	1×10^{14}	1×10^{14}	1×10^{14}	1×10^{14}	1×10^{14}	1×10^{14}	1×10^{14}

Figure 4(a) depict energy band diagram of $CsSn_{0.5}Ge_{0.5}I_3$ based PSC device with PEDOT: PSS as HTL and ZnO as ETL. For PEDOT: PSS as HTL, VBO obtained with this absorber is -0.4 eV.CBO for ZnO is found -0.1 eV. Fig. 4(b) depict Energy band diagram of $CsSn_{0.5}Ge_{0.5}I_3$ based PSC device with PEDOT: PSS as HTL and TiO_2 as ETL. CBO for $TiO_2$is found -0.1 eV. Fig. 4(c) depict energy band diagram of $CsSn_{0.5}Ge_{0.5}I_3$ based PSC device with PEDOT: PSS as HTL and WS_2 as ETL. CBO for $WS_2$is found -0.05 eV. Fig. 4(d) depict energy band diagram of $CsSn_{0.5}Ge_{0.5}I_3$ based PSC device with PEDOT: PSS as HTL and PCBM as ETL. CBO for PCBM is found 0 eV. Fig. 4(e) depict Energy band diagram of $CsSn_{0.5}Ge_{0.5}I_3$ based PSC device with PEDOT: PSS as HTL and C_{60} as ETL. CBO for C_{60} is also found 0 eV. It is well observed that all CBO and VBO of devices is falling in prescribed range.

5.3. Effect of Joint variation ETL and PAL

Joint variation of thickness of ETL and PAL has been studied for all five best devices for getting specific optimum design parameters. ETL and PAL width of all five PSCs varied from 200 nm to 1400 nm and its effect has been observed on solar cell parameters namely V_{OC}, J_{SC}, FF and PCE. Effect of joint width variation of ETL and HTL on V_{OC} for all five devices has been shown in Fig. 5 in which contour of V_{OC} is plotted for all five PSCs ITO/(ZnO,TiO_2,WS_2,PCBM,C_{60})/$CsSn_{0.5}Ge_{0.5}I_3$/ PEDOT: PSS/Au.

Keeping PAL thickness constant at 200nm and varying ETL thickness from 200nm to 1400nm, ZnO based PSC provided constant value of V_{OC}1.16 volt, TiO_2 based PSC given value of V_{OC} 1.16 volt, WS_2 based PSC provided V_{OC} 1.17 volt, PCBM based PSC provided V_{OC} 1.16 volt up to 600nm of width of ETL but reduced slightly after that, at 1400nm of width it provided value of V_{OC} as 1.14 volt. C_{60} based PSC provided V_{OC} 1.14 volt at 200nm of width of ETL but reduced slightly after that, at 1400nm of width it provided value of V_{OC} 1.07 volt. Further, increasing PAL thickness from 200nm to 1400nm contributed significant reduction in V_{OC} for all the ETL combinations. This occurred mainly due to increased recombination of carriers in absorber layer. At 1400 nm of width of PAL, ZnO based PSC provided V_{OC} 1.07 volt, TiO_2 based PSC given V_{OC} 1.07 volt,WS_2 based PSC provided V_{OC} 1.07 volt, PCBM based PSC provided V_{OC} 1.07 volt and C_{60} based PSC provided V_{OC} 1.05 volt.

Effect of joint width variation of ETL and HTL on J_{SC} for all five devices has been shown in Fig. 6. in which contour of J_{SC} (mA/cm^2) is plotted for all

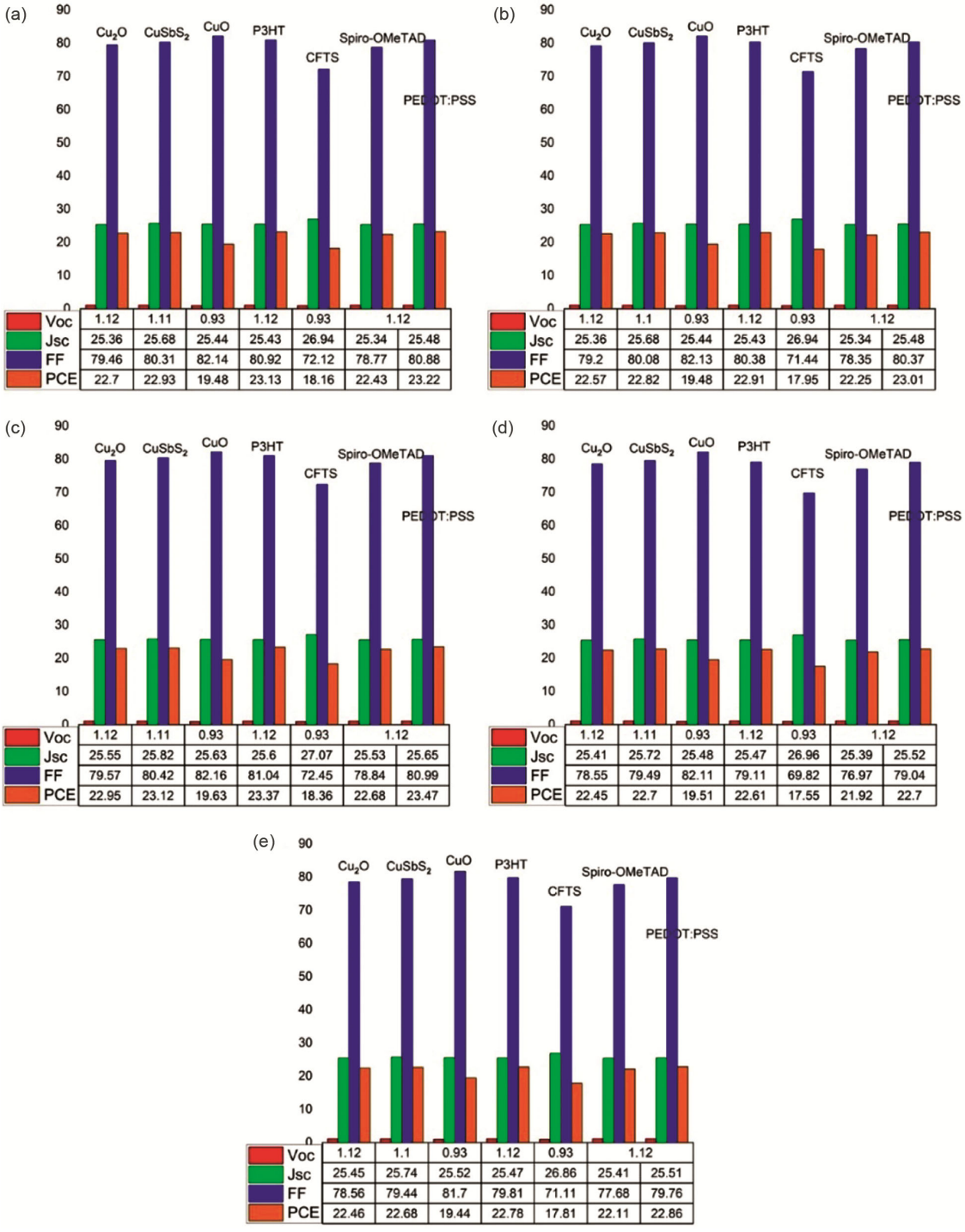

Fig. 3 — Solar cell parameters of $CsSn_{0.5}Ge_{0.5}I_3$-based PSC device for various HTLs with Au as back contact and (a) ZnO (b) TiO_2 (c) WS_2 (d) PCBM and (e) C_{60} as the ETL

five PSCs ITO/(ZnO, TiO_2, WS_2, PCBM, C_{60})/ $CsSn_{0.5}Ge_{0.5}I_3$/PEDOT:PSS/Au.

Keeping PAL thickness constant at 200nm and varying ETL thickness from 200nm to 1400nm, ZnO based PSC provided nearly constant value of J_{SC} 19.38 (mA/cm^2),TiO_2 based PSC given value of J_{SC} 19.38 (mA/cm^2) for nearly all width of ETL, at 200nm width of ETL. WS_2 based PSC provided J_{SC} 21.52 (mA/cm^2) which increases with increase in width of ETL and given J_{SC} 21.52 (mA/cm^2) at 1400nm. PCBM

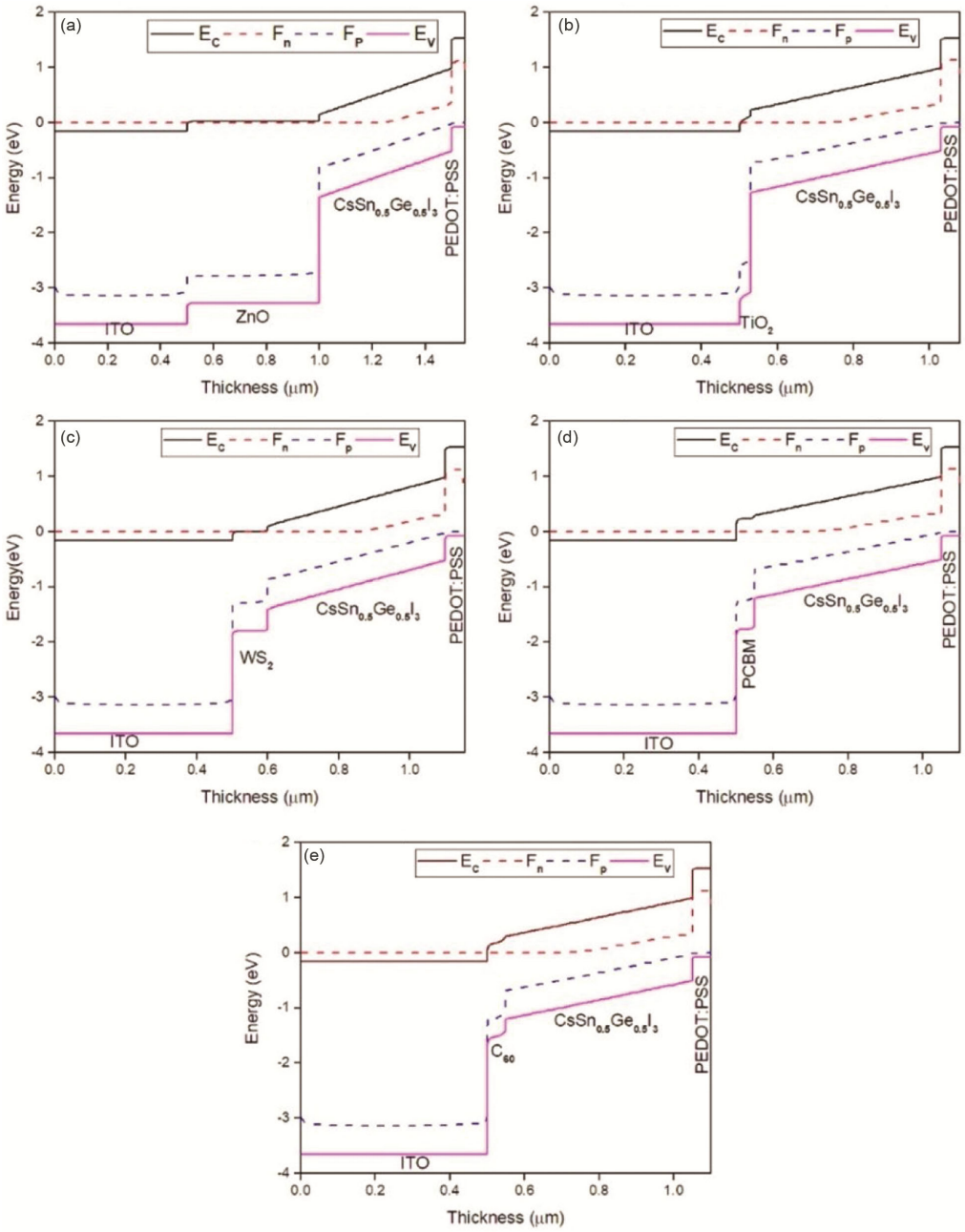

Fig. 4 — Energy diagram of $CsSn_{0.5}Ge_{0.5}I_3$ based PSC device with PEDOT: PSS as HTL and (a) ZnO (b) TiO_2 (c) WS_2 (d) PCBM and (e) C_{60} as ETL

based PSC provided J_{SC} 20.46(mA/cm^2) at 200nm of width of ETL but reduced drastically after that, at 1400nm of width it provided value of J_{SC} 12.33 (mA/cm^2), C_{60} based PSC provided J_{SC} 16.28 (mA/cm^2) at 200nm of width of ETL but reduced drastically after that, at 1400nm of width it provided value of J_{SC} 2.75 (mA/cm^2). Further, increasing PAL thickness from 200nm to 1400nm contributed increase in J_{SC} up to nearly 600nm width, then after it become nearly constant for all the ETLs combinations. This occurred mainly due to increase in carrier generation due to more thickness and absorption of more photon but recombination of carriers produced counter effect that causes current to become constant after a certain optimum width. At 1400 nm of width of PAL and 200nm width of ETL, ZnO based PSC provided J_{SC} 28.07 (mA/cm^2), TiO_2 based PSC given J_{SC} 28.07 (mA/cm^2),WS_2 based PSC

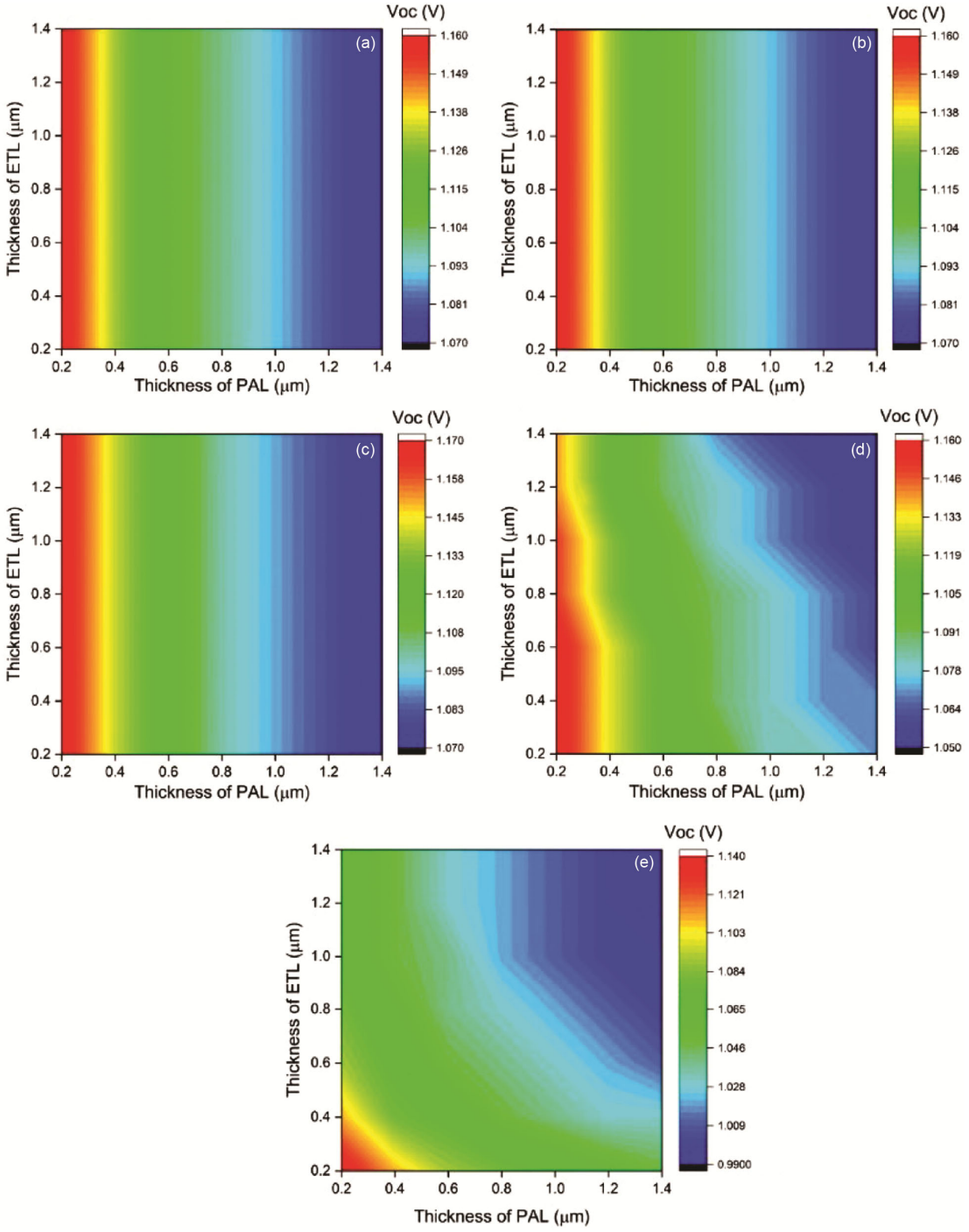

Fig. 5 — Showing the Contour graph of V_{OC} (V) as a joint function of thickness of PAL and thickness of (a) ZnO (b) TiO_2 (c) WS_2 (d) PCBM and (e) C_{60} as the ETL

provided J_{SC} 28.07 (mA/cm^2), PCBM based PSC provided J_{SC} 27.86 (mA/cm^2) and C_{60} based PSC provided J_{SC} 20.67 (mA/cm^2).

Effect of joint width variation of ETL and HTL on FF for all five devices has been shown in Fig. 7 in which contour of FF (%) is plotted for all five PSCs ITO/(ZnO, TiO_2, WS_2, PCBM, C_{60})/$CsSn_{0.5}Ge_{0.5}I_3$/PEDOT:PSS/Au.

Keeping PAL thickness constant at 200nm and varying ETL thickness from 200nm to 1400nm, ZnO based PSC provided constant value of FF 80.88%, TiO_2 based PSC given value of FF 80.12%,WS_2 based

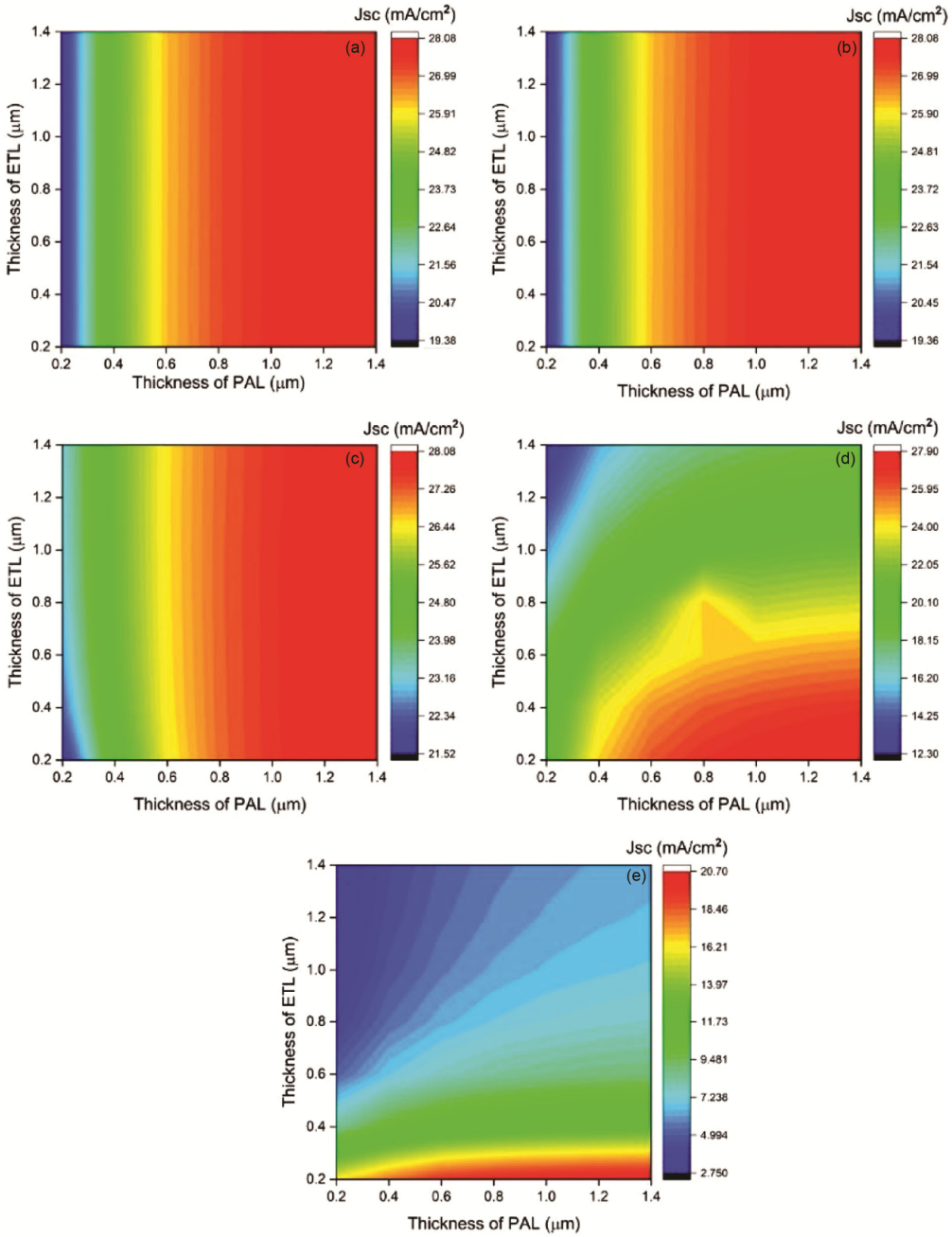

Fig. 6 — Showing the Contour graph of J_{SC} (mA/cm^2) as a joint function of thickness of PAL and thickness of (a) ZnO (b) TiO_2 (c) WS_2 (d) PCBM and (e) C_{60} as the ETL

PSC provided FF 81.84% which increases slightly with increase in width of ETL, at 1400 nm of width it provided FF 82.23%, PCBM based PSC provided FF 78.74% but reduced slightly and at 1400nm of width it provided value of FF 76.64%.C_{60} based PSC provided FF 70.82% at 200nm of width of ETL but reduced drastically and at 1400nm of width it provided value of FF 56.1%. Further, increasing PAL thickness from 200nm to 1400nm contributed reduction in FF for all the ETLs combinations. This occurred mainly due to decreased open circuit voltage and increased absorber area. At 1400 nm of width of PAL, ZnO based PSC provided FF 78.46%, TiO_2 based PSC given FF 78.15%, WS_2 based PSC provided FF 78.53%, PCBM based PSC provided FF 77.58% and C_{60} based PSC provided FF 77.53%.

Effect of joint width variation of ETL and HTL on PCE for all five devices has been shown in Fig. 8 in

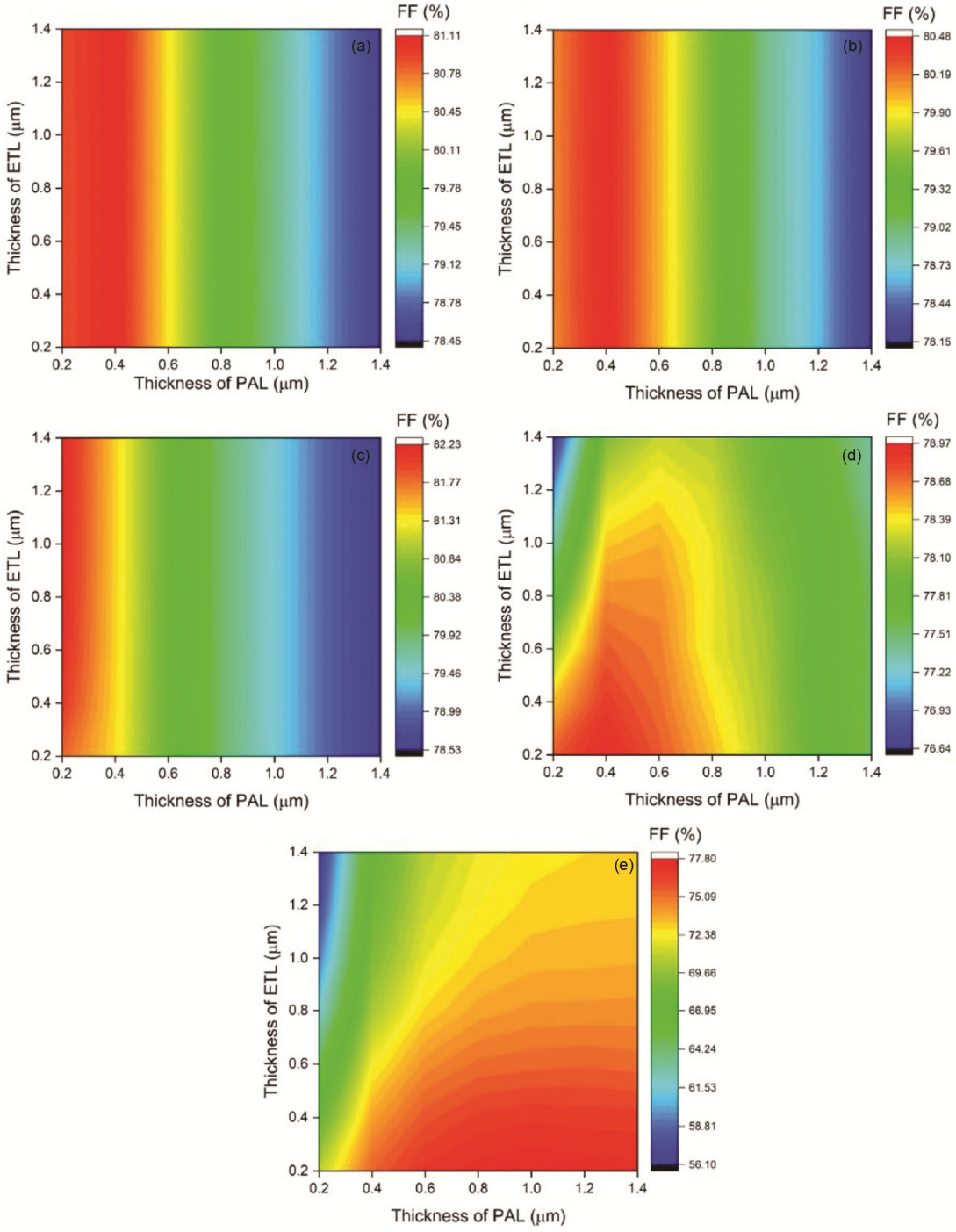

Fig. 7 — Showing the Contour graph of FF(%) as a joint function of thickness of PAL and thickness of (a) ZnO (b) TiO_2 (c) WS_2 (d) PCBM and (e) C_{60} as the ETL

which contour of PCE (%) is plotted for all five PSCs ITO/(ZnO,TiO_2,WS_2,PCBM,C_{60})/$CsSn_{0.5}Ge_{0.5}I_3$/PEDOT:PSS/Au.

Keeping PAL thickness constant at 200nm and varying ETL thickness from 200nm to 1400nm, ZnO based PSC provided nearly constant value of PCE 18.26%,TiO_2 based PSC given value of PCE nearly 18.01% at all the width of ETL. At 200nm width of ETL, WS_2 based PSC provided PCE 20.7% which increases with increase in width of ETL and given PCE 22.45 % at 1400 nm. PCBM based PSC provided PCE 18.8 % at 200nm of width of ETL but reduced

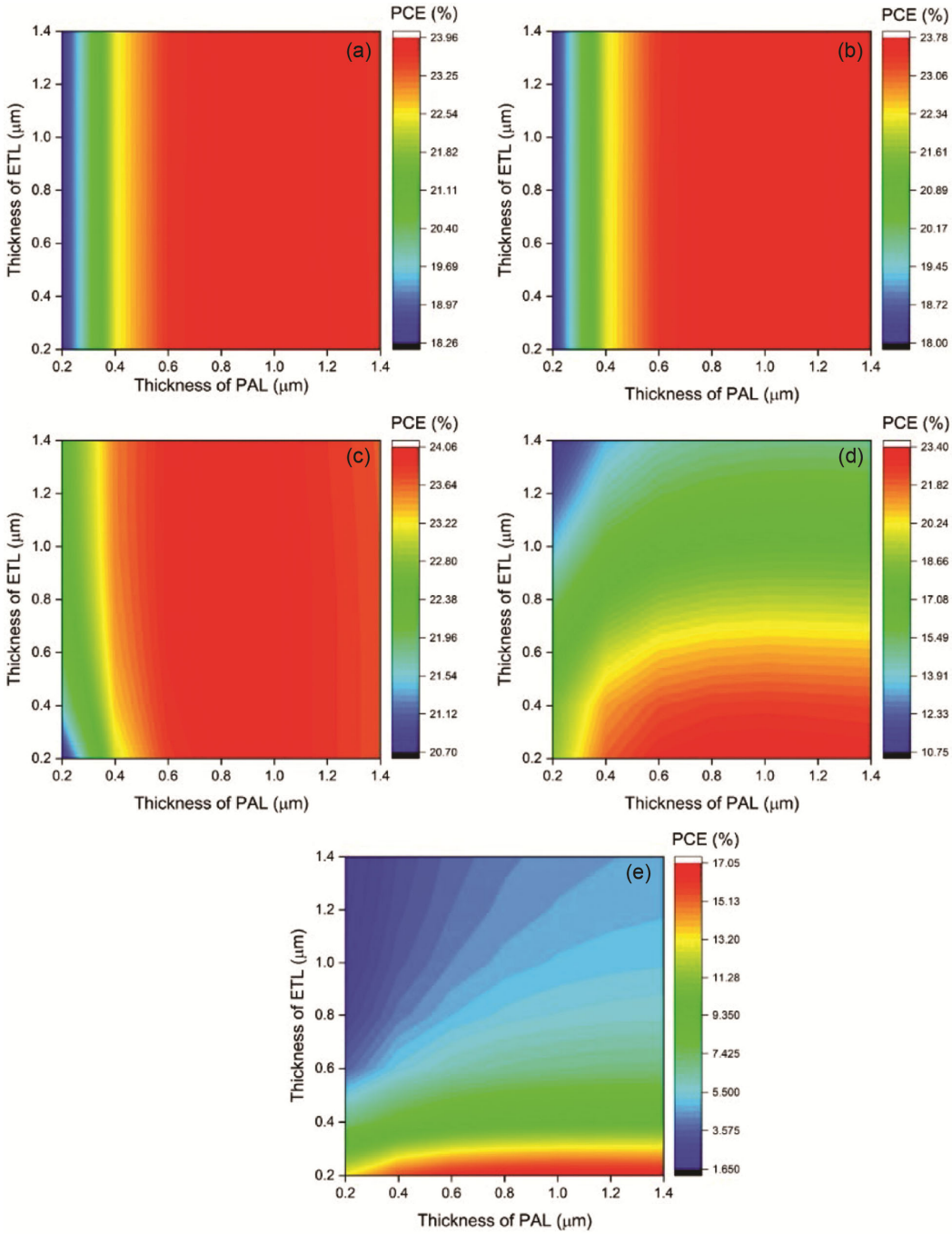

Fig. 8 — Showing the Contour graph of PCE(%) as a joint function of thickness of PAL and thickness of (a) ZnO (b) TiO_2 (c) WS_2 (d) PCBM and (e) C_{60} as the ETL

drastically and at 1400nm of width it provided value of PCE 10.79 %, C_{60} based PSC provided PCE 13.22 % at 200nm of width of ETL but reduced drastically and at 1400nm of width it provided value of PCE 1.66 %. Further, increasing PAL thickness from 200nm to 1400nm contributed increase in PCE up to nearly 600nm width, then after it become nearly constant for all the ETLs combinations. This occurred mainly due to more thickness allow absorption of more photon that causes increase in carrier generation but recombination of carriers produced counter effect that causes current to become constant after a certain optimum width. At 1400 nm of width of PAL and 200nm width of ETL, ZnO based PSC provided PCE

28.07 %, TiO_2 based PSC given value of PCE 23.55 %, WS_2 based PSC provided PCE 23.72 %. PCBM based PSC provided PCE 23.18 % and C_{60} based PSC provided PCE 16.94 %.

From aforesaid result it can be concluded that for the ZnO and TiO_2 based PSC, ETL width variation has very less effect. But for WS_2 based PSC increase in ETL width causes to enhancement of solar cell parameters while for PCBM and C_{60} based PSC increase in ETL width causes reduction in solar cell parameters.

Table 6 shows simulation results of the best HTL i.e. PEDOT: PSS with different ETLs at optimized thickness of ETL, HTL and PAL. In comparison to all other PSCs ITO/WS_2/$CsSn_{0.5}Ge_{0.5}I_3$/PEDOT: PSS/Au provided best possible solar cell parameters.

5.4 Effect of variations of Series resistance, Shunt resistance and Temperature on PSC parameters

Equivalent equation of current with series and shunt resistance in PSCs is shown as

$$i = I_g - \frac{V + R_s i}{R_{sh}} - I_s[e^{\frac{V+R_s i}{\eta V_T}} - 1]$$

where, i = current of cell, V = voltage of cell, R_S = series resistance, R_{Sh} = shunt resistance, I_g = photogenerated current, V_T = Thermal voltage, η = ideality factor of cell.

A lower series resistance and higher value of shunt resistance is required for high value of J_{SC} and PCE. Series resistance has direct effect on FF and J_{SC}. Fig. 9 shows variation of Solar cell parameters with series resistance. Here the R_S is varied from 0-6 Ω-cm^2 with

Table 6 — Simulation results of the best HTL with different ETLs.

Device structure	V_{OC} (V)	J_{SC} (mA/cm^2)	FF (%)	PCE (%)
ITO/ZnO/$CsSn_{0.5}Ge_{0.5}I_3$/PEDOT:PSS/Au	1.12	25.48	80.88	23.22
ITO/TiO_2/$CsSn_{0.5}Ge_{0.5}I_3$/PEDOT:PSS/Au	1.12	25.48	80.37	23.01
ITO/WS_2/$CsSn_{0.5}Ge_{0.5}I_3$/PEDOT:PSS/Au	1.12	25.65	80.99	23.47
ITO/PCBM/$CsSn_{0.5}Ge_{0.5}I_3$/PEDOT:PSS/Au	1.12	25.52	79.04	22.7
ITO/C_{60}/$CsSn_{0.5}Ge_{0.5}I_3$/PEDOT:PSS/Au	1.12	25.51	79.76	22.86

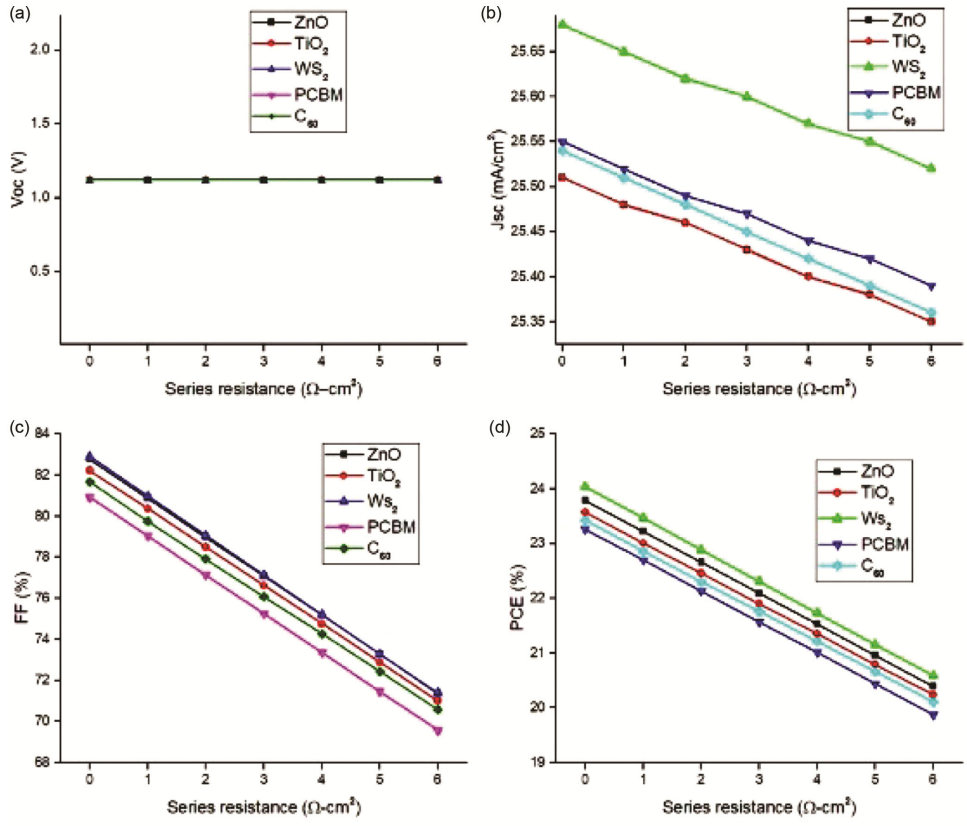

Fig. 9 — Effect of series resistance (R_S) on (a) V_{OC}, (b) J_{SC}, (c) FF, and (d) PCE for different ETLs with PEDOT: PSS as HTL when R_{Sh} = 10^3 Ω-cm^2.

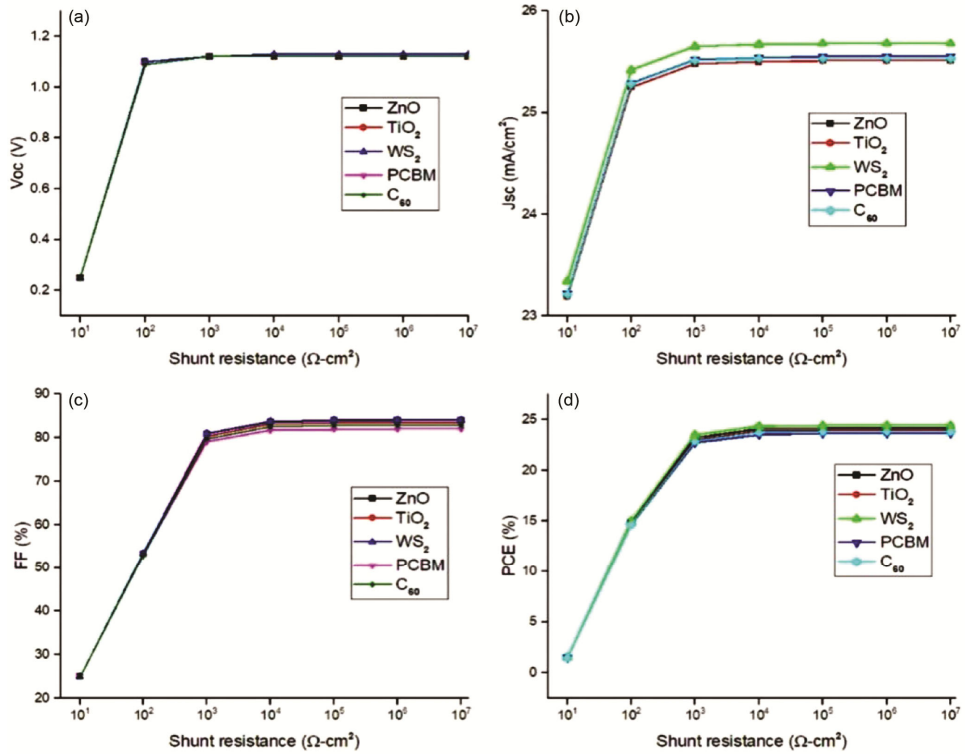

Fig.10 — Effect of shunt resistance (R_{SH}) on (a) V_{OC}, (b) J_{SC}, (c) FF and (d) PCE for different ETLs with PEDOT: PSS as HTL when R_S = 1 Ω-cm^2

the value of R_{Sh} fixed at 10^3 Ω-cm^2. V_{OC} for solar cells for different ETL combinations remain constant whereas V_{OC}, J_{SC}, FF and PCE reduced linearly with enhancement in series resistance for all the combinations of solar cells.

Figure 10 depict the variation of solar cell parameters of all combinations pf PSCs with the shunt resistance. All parameters show improvement with increase in shunt resistance. R_{Sh} is varied from10^1-10^7 Ω-cm^2 with the value of R_S fixed at 1 Ω-cm^2.For the value of R_{Sh}<1E+04 all the parameters V_{OC}, J_{SC}, FF and PCE increase with the increase in the value of shunt resistance. For the value of Rsh>1E+04 all parameter V_{OC}, J_{SC}, FF and PCE remain constant.

Figure 11 Shows variation in solar cell parameters (a) V_{OC}, (b) J_{SC}, (c) FF and (d) PCE for different ETLs with PEDOT: PSS as HTL with respect to temperature. Increase in temperature causes generation of more number of electron hole pairs in absorber but also produce counter effect, it increases ions vibration and collisions that obstruct free flow of carriers *i.e.* decrease mobility and hence current density J_{SC} become nearly constant for all the combination of PSCs. Further temperature has adverse effect on V_{OC}, FF and PCE. They decrease sharply with increase in temperature for all the PSCs.

Increase in temperature reduce the bandgap of perovskite material, which in turn reduce open circuit voltage V_{OC}. Increase in temperature increases reverse saturation current density J_O. Governing equation for V_{OC} is given below as:-

$$V_{OC} = \frac{nK_AT}{q}\left[\ln\left(1+\frac{J_{SC}}{J_O}\right)\right]$$

Where, $\frac{K_AT}{q}$ = Thermal voltage and n = ideality factor and J_O = Reverse saturation current density.

Here from above equation it can be inferred that increase in J_O causes decrease in V_{OC}.

5.5 J-V and QE Characteristics

Under a 1.5 AM illumination, the J-V characteristics of the five PSCs are shown in Fig. 12(a). It can be inferred that C_{60} as ETL has given inferior J-V characteristics in comparison to ZnO, TiO_2,WS_2 and PCBM. In all the devices WS_2 displays the best J-V characteristics. QE for all the PSCs is plotted in Fig. 12(b). At 400nm wavelength of QE tend to unity for all the ETLs after that it reduces slowly up to 700 nm then after that it drop

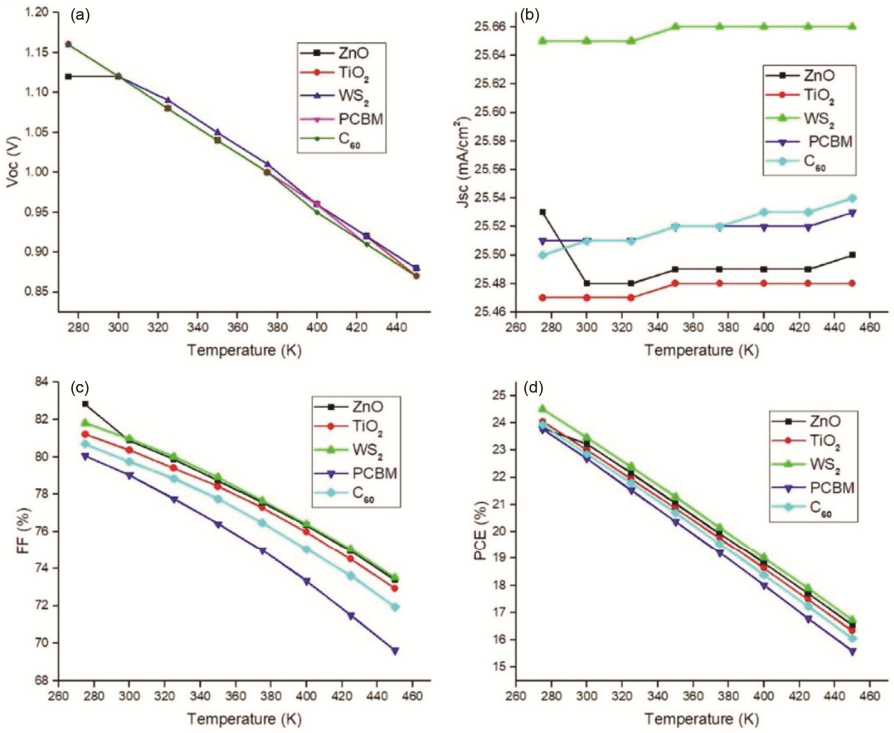

Fig. 11 — Effect of temperature on (a) V_{OC}, (b) J_{SC}, (c) FF and (d) PCE for different ETLs with PEDOT: PSS as HTL

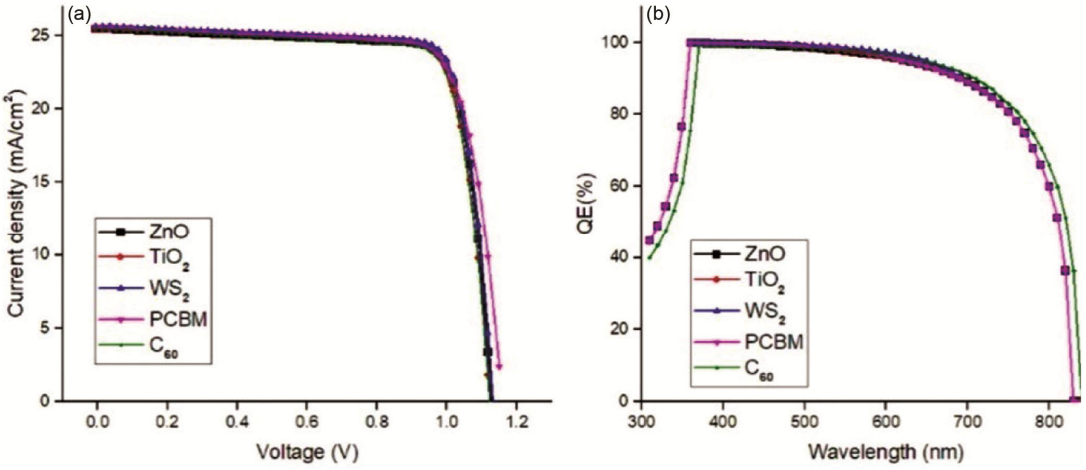

Fig. 12 — Effect of (a) J-V and (b) Q-E for different ETLs with PEDOT: PSS as HTL

sharply. WS_2 shows superior QE in comparison to all other ETL PSCs.

Performance of PSCs are generally assessed and determined by J-V characteristics. J-V characteristics plots current density (J) as a function of Voltage (V) of the solar cell. Many solar cell parameters could be obtained from the J-V characteristic like V_{OC}, J_{SC}, current density (J_{mp}) and the voltage (V_{mp}) at the maximum power point. Fig 12(a) shows J-V characteristics for all the five PSCs. From JV plot it can be inferred that J_{SC} is about 25 mA/cm^2 and V_{OC} is about 1.1 volt for all the PSCs. It can be concluded that C_{60} based PSC has shown inferior J-V characteristics in comparison to ZnO, TiO_2, WS_2 and PCBM based PSCs. In all the devices WS_2 displays the best J-V characteristics.

The solar cell's quantum efficiency(QE) shows the percentage of incoming photons at a specific wavelength that are transformed to charge carriers *i.e.* electrons and holes. The quantum efficiency graphs of different structures have been shown in the Fig. 12(b). For ideal conditions, QE for a particular wavelength is

Table 7 — Comparison of the simulation results of wxAMPS and SCAPS-1D for the HTL PEDOT: PSS

Device structure	Software	Voc (V)	Jsc (mA/cm^2)	FF (%)	PCE (%)
ITO/ZnO/$CsSn_{0.5}Ge_{0.5}I_3$/PEDOT:PSS/Au	wxAMPS	1.12	25.74	79.97	23.20
	SCAPS-1D	1.12	25.48	80.88	23.22
ITO/TiO_2/$CsSn_{0.5}Ge_{0.5}I_3$/PEDOT:PSS/Au	wxAMPS	1.12	27.07	79.87	24.33
	SCAPS-1D	1.12	25.48	80.37	23.01
ITO/WS_2/$CsSn_{0.5}Ge_{0.5}I_3$/PEDOT:PSS/Au	wxAMPS	1.13	27.10	80.23	24.59
	SCAPS-1D	1.12	25.65	80.99	23.47
ITO/PCBM/$CsSn_{0.5}Ge_{0.5}I_3$/PEDOT:PSS/Au	wxAMPS	1.11	22.64	78.82	19.95
	SCAPS-1D	1.12	25.52	79.04	22.70
ITO/C_{60}/$CsSn_{0.5}Ge_{0.5}I_3$/PEDOT:PSS/Au	wxAMPS	1.11	23.62	78.45	20.72
	SCAPS-1D	1.12	25.51	79.76	22.86

5.7 Comparison of this work with earlier works

Table 8 — Comparison of the simulation results of different works done

Device Structure	V_{OC}(V)	J_{SC} (mA/cm^2)	FF(%)	PCE(%)	References
FTO/PCBM/$CsSn_{0.5}Ge_{0.5}I_3$/ Spiro-OMeTAD/Au	0.87	27.05	79.25	18.79	[33]
FTO/PC60BM/ $CsSn_{0.5}Ge_{0.5}I_3$/Spiro-OMeTAD/Au	1.115	28.70	87.86	18.13	[34]
FTO/WS_2/$CsSn_{0.5}Ge_{0.5}I_3$/ MoS_2/Au	0.96	27.3	87.62	22.17	[35]
FTO/PCBM/$CsSn_{0.5}Ge_{0.5}I_3$/Spiro-OMeTAD/Au	0.63	18.61	0.606	7.11	[24]
$CsSn_{0.5}Ge_{0.5}I_3$	0.64	15.82	73.63	7.45	[36]
ITO/ZnO/$CsSn_{0.5}Ge_{0.5}I_3$/Spiro-OMeTAD/Au	0.97	29.56	84.15	21.27	[37]
ITO/ZnO/$CsSn_{0.5}Ge_{0.5}I_3$/PEDOT:PSS/Au	1.12	25.48	80.88	23.22	This Work
ITO/TiO_2/$CsSn_{0.5}Ge_{0.5}I_3$/PEDOT:PSS/Au	1.12	25.48	80.37	23.01	This Work
ITO/WS_2/$CsSn_{0.5}Ge_{0.5}I_3$/PEDOT:PSS/Au	1.12	25.65	80.99	23.47	This Work
ITO/PCBM/$CsSn_{0.5}Ge_{0.5}I_3$/PEDOT:PSS/Au	1.12	25.52	79.04	22.7	This Work
ITO/C_{60}/$CsSn_{0.5}Ge_{0.5}I_3$/PEDOT:PSS/Au	1.12	25.51	79.76	22.86	This Work

1. Here QE value with respect to different wavelengths for the absorber $CsSn_{0.5}Ge_{0.5}I_3$ with same HTL and different ETLs has been obtained. QE value for all the ETLs PSCs approaches towards unity at 400 nm wavelength after that it reduces slowly up to 700 nm then after that it drop sharply.WS_2 based PSC shows superior QE in comparison to all other ETL PSCs.

5.6 Comparison of SCAPS 1D and wxAMPS Results

A thorough secondary verification of results for all the PSCs has been obtained in another software wxAMPS and comparison of simulation results with SCAPS-1D is shown in Table 7. Results of solar cell parameters obtained in wxAMPS is found nearly equal to result given by SCAPS-1D Software. ZnO, PCBM and C_{60} based PSCs have provided less PCE in wxAMPS as compared to SCAPS 1D whereas TiO_2 and WS_2 based PSCs have provided more PCE in wxAMPS as compared to SCAPS 1D. Table 8 presents the enhanced outcomes as compared to the previous studies.

6 Conclusion

In the present work feasibility of perovskite absorber $CsSn_{0.5}Ge_{0.5}I_3$ using alloy of group 4 elements Sn and Cs as a replacement of toxic lead is studied extensively. 35 different device structure with different ETL and HTL combinations has been accomplished for obtaining efficient and stable lead free PSC. Among all HTLs PEDOT: PSS has provided highest solar cell parameters like V_{OC}, J_{SC}, FF and PCE with all other combinations of ETLs. Five distinct devices with PEDOT: PSS as HTL**,** $CsSn_{0.5}Ge_{0.5}I_3$ as PAL and different ETLs have been thoroughly studied and analyzed for different design parameters like ETL and PAL width variations, effect of input and output resistances and effect of temperature. All PSCs have been simulated using SCAPS-1D software and cross validated with another simulation software wxAMPS. Also simulation result using these software has been validated with experimental result for same absorber. The device structure ITO/WS_2/$CsSn_{0.5}Ge_{0.5}I_3$/PEDOT: PSS/Au provided superior solar cell parameters among all five PEDOT: PSS based devices. This PSC provided best possible PCE of 23.47%, V_{OC} of 1.12 volt, J_{SC} of 25.65 (mA/cm^2) and FF of 80.99%.This is mainly due to increased charge carrier pairs generation and reduced recombination respectively. The present study will contribute towards the fabrication of highly efficient environment friendly lead free $CsSn_{0.5}Ge_{0.5}I_3$ based PSCs**.**

References

1 Noel N K, Stranks S D, Abate A, Wehrenfennig C, Guarnera S, Haghighirad A A, Sadhanala A, Eperon G E, Pathak S K, Johnston M B, Petrozza A, Herz L M & Snaith H J, *Energy Environ Sci*, 7 (2014) 3061.

2 Tai Q D, Tang K C & Yan F, *Energy Environ Sci*, 12 (2019) 2375.

3 Wang R, Mujahid M, Duan Y, Wang Z K, Xue J J & Yang Y, *Adv Funct Mater*, 29 (2019) 180884.

4 Kojima A, Teshima K, Shirai Y & Miyasaka T, *J Amer Chem Soc*, 131 (2009) 6050.

5 Green M A, Ho-Baillie A & Snaith H J, *Nature Photon*, 8 (2014) 506.

6 Kim G, Min H, Lee K S, Lee D Y, Yoon SM & Seok S I, *Science*, 370 (2020) 108.

7 Jiang Q , Zhao Y , Zhang X , Yang X, Chen Y , Chu Z , Ye Q , Li X , Yin Z & You J, *Nature Photon*, 13 (2019) 460.

8 Yang W S, Park B-W, Jung E H, Jeon N J, Kim Y C, Lee D U, Shin S S, Seo J, Kim E K, Noh J H & Seok S I, *Science*, 356 (2017) 1376.

9 Miyata A, Mitioglu A, Plochocka P, Portugall O, Wang J T-W , Stranks S D, Snaith H J & Nicholas R J, *Nat Phys*, 11 (2015) 582.

10 Chen B, Yang M, Priya S & Zhu K, *J Phys Chem Lett*, 7 (2016) 905.

11 Grätzel M, *Nat Mater,* 13 (2014) 838.

12 Ju M G, *et al*., *Joule*, 2 (2018) 1231.

13 Zong Y, *et al*., *Chem*, 4 (2018) 1404.

14 Ahmed S, Gondal M A, Alzahrani A S, Parvaz M, Ahmed A & Hussain S, *ACS Appl Energy Mater*, 7 (2024) 1382.

15 Krishnamoorthy T, *et al*., *J Mater Chem A*, 3 (2015)23829.

16 Bala N, *et al*., *Indian J Pure Appl Phys*, 62 (2024) 292.

17 Hao F, Stoumpos C C, Cao D H, Chang R P H & Kanatzidis M G, *Nat Photon*, 8 (2014) 489.

18 Shao S, *et al*., *Adv Energy Mater*, 8 (2018) 1702019.

19 Dang Y, *et al*., *Angew Chem Int Ed*, 55 (2016) 3447.

20 Zhou Y, *et al*., *J Mater Chem A*, 4 (2016) 17623.

21 Wu B, *et al.*, *Adv Funct Mater*, 27 (2017) 1604818.

22 Noel N K, Stranks S D, Abate A, Wehrenfennig C, Guarnera S, Haghighirad A-A, Sadhanala A, Eperon G E, Pathak S K, Johnston M B, Petrozza A, Herz L M & Snaith H J, *Energy Environ Sci*, 7 (2014) 3061.

23 Kumar R, Kim G, Karupannan H-J & Prabakar S K, *J Phys Chem C*, 121 (2017) 16447.

24 Chen M, Ju M G, Garces H F, Carl A D, Ono L K, Hawash Z, Zhang Y, Shen T, Qi Y, Grimm R L, Pacifici D, Zeng X C, Zhou Y & Padture N P, *Nat Commun*, 10 (2019). 10.1038/s41467-018-07951-y.

25 Singh N, Agarwal A & Agarwal M, *Opt Mater*, 114 (2021) 110964.

26 Alam I, Mollick R & Ashraf M A, *Phys B*, 618 (2021) 413187.

27 Gong J, Darling S B & You F, *Energy Environ Sci*, 8 (2015) 1953.

28 Choi H, Park S, Paek S, Ekanayake P, Nazeeruddin M K & Ko J, *J Mater Chem A*, 2 (2014) 19136.

29 Devi C & Mehra R, *J Mater Sci*, 54 (2019) 5615.

30 Hossain M K, Rubel M H K, Toki G F I, Alam I, Rahman Md. F & Bencherif H, *ACS Omega*, 7 (2022) 43210.

31 Islam M T, Jani Md. R, Islam A F, Shorowordi K Md, Chowdhury S, Nishat S S & Ahmed S, *IEEE Trans Electron Dev*, 68 (2021) 618.

32 Basyoni M S S, Salah M M, Mousa M, Shaker A, Zekry A, Abouelatta M, Alshammar M T, Al-Dhlan K A & Gontrand C, *IEEE Access*, 9 (2021) 130221.

33 Nalianya M A, Awino C, Barasa H, Odari V, Gaitho F, Omogo B & Mageto M, *Optik*, 248 (2021) 168060.

34 Bouazizi S, Tlili W, Bouich A, Soucase B M & Omri A, *Mater Res Express*, 9 (2022) 096402.

35 Kaity A, Shubham, Singh S & Pandey S K, *Superlatt Microstruct*, 156 (2021) 106972.

36 Islam Md. T, Jani Md. R, Islam A F, Shorowordi K Md., Chowdhury S, Nishat S S & Ahmed S, *IEEE Trans Electron Dev*, 68 (2021) 618.

37 Bhatt S, Shukla R, Pathak C & Pandey S K, *Solar Energy*, 215 (2021) 473.